Mon. Not. R. Astron. Soc. **374,** 323–336 (2007) doi:10.1111/j.1365-2966.2006.11150.x

Clues for the origin of the fundamental metallicity relations – I. The hierarchical building up of the structure

Maria E. De Rossi,[1,2] Patricia B. Tissera[1,2⋆] and Cecilia Scannapieco[1,2]

[1]*Consejo Nacional de Investigaciones Científicas, y Técnicas, Rivadavia 1917, (1428) Buenos Aires, Argentina*
[2]*Instituto de Astronomía. y Física del Espacio, Argentina, CC67 Suc28, Buenos Aires (1428), Argentina*

Accepted 2006 October 3. Received 2006 September 28; in original form 2006 July 6

ABSTRACT

We analyse the evolutionary history of galaxies formed in a hierarchical scenario consistent with the concordance Lambda cold dark matter (ΛCDM) model focusing on the study of the relation between their chemical and dynamical properties. Our simulations consistently describe the formation of the structure and its chemical enrichment within a cosmological context. Our results indicate that the luminosity–metallicity and the stellar mass–metallicity (LZR and MZR) relations are naturally generated in a hierarchical scenario. Both relations are found to evolve with redshift. In the case of the MZR, the estimated evolution is weaker than that deduced from observational works by approximately 0.10 dex. We also determine a characteristic stellar mass, $M_{\rm c} \approx 3 \times 10^{10}$ M$_\odot$, which segregates the simulated galaxy population into two distinctive groups and which remains unchanged since $z \sim 3$, with a very weak evolution of its metallicity content. The value and role played by $M_{\rm c}$ is consistent with the characteristic mass estimated from the SDSS galaxy survey by Kauffmann et al. Our findings suggest that systems with stellar masses smaller than $M_{\rm c}$ are responsible for the evolution of this relation at least from $z \approx 3$. Larger systems are stellar dominated and have formed more than 50 per cent of their stars at $z \geqslant 2$, showing very weak evolution since this epoch. We also found bimodal metallicity and age distributions from $z \sim 3$, which reflects the existence of two different galaxy populations. Although SN feedback may affect the properties of galaxies and help to shape the MZR, it is unlikely that it will significantly modify $M_{\rm c}$ since, from $z = 3$ this stellar mass is found in systems with circular velocities larger than 100 km s^{-1}.

Key words: galaxies: abundances – galaxies: evolution – galaxies: formation – cosmology: theory.

1 INTRODUCTION

Chemical abundances could provide important clues on the evolutionary history of galaxies (e.g. Freeman & Bland-Hawthorn 2002) since they are the result of the joint action of several physical processes such as supernova (SN) feedback (Larson 1974; Larson & Dinerstein 1975; White & Rees 1978; Kauffmann & Charlot 1998; Somerville & Primack 1999; Cole et al. 2000; Springel & Hernquist 2003), gas inflow (Pagel 1997), mergers and interactions, among others. Moreover, although it is not easy to disentangle the effect of each individual process, it may be possible to constrain galaxy formation models by studying how chemical and dynamical properties of galaxies evolve as a function of cosmic epoch (Pettini 2006) and confronting them with observations.

There are strong evidences for the existence of a good correlation between the luminosities of local galaxies and their chemical abundances which show that metallicities tend to increase with galaxy luminosity. In addition, recent studies have suggested that the luminosity–metallicity relation (LZR) evolves with redshift so that, at a given metallicity, galaxies were brighter in the past (Pettini et al. 2001; Kobulnicky et al. 2003; Kobulnicky & Kewley 2004; Lamareille et al. 2004; Maier, Meisenheimer & Hippelein 2004; Shapley et al. 2004). An evolution in both the zero-point and the slope is suggested, indicating a differential evolution in the chemical content of the systems as a function of luminosity. In particular, in agreement with previous works, Kobulnicky & Kewley (2004), found that the largest change from $z \sim 3$ is driven by faint galaxies, while from $z \sim 1$, they detected an increase in the metallicity level of ∼0.14 dex. Interestingly, Erb et al. (2006a) showed that the large uncertainties present in the determination of the LZR at high redshift, introduced mainly by the variations in the mass-to-light ratios, make it very difficult to draw a robust conclusion on its evolution.

Luminosities are normally used as a surrogate of stellar mass because of the difficulty in measuring the latter. However, it is now accepted that the correlation between metallicity and stellar mass is

⋆E-mail: patricia@iafe.uba.ar

more fundamental. This correlation was first reported by Lequeux et al. (1979) in a study of irregular galaxies. Recently, Tremonti et al. (2004, hereafter T04) confirmed this correlation on a statistical basis by determining a tight correlation between gas-phase metallicity and stellar mass, extended over a factor of 10 in metallicity and three decades in stellar mass, for a sample of ≈30 000 local star-forming galaxies in the Sloan Digital Sky Survey (SDSS). The stellar mass–metallicity (MZR) shows a linear growth between $10^{8.3}$ and $10^{10.35}$ $M_\odot\ h^{-1}$, flattening for larger stellar mass. T04 interpreted this behaviour as the efficient action of galactic winds over systems with masses lower than $\sim 10^{10.35}$ $M_\odot\ h^{-1}$. This stellar mass has been previously identified as a characteristic mass for galaxy evolution (Kauffmann et al. 2004). Furthermore, Gallazzi et al. (2005, hereafter G05) analysed stellar masses, light-weighted ages and stellar metallicities for a sample of galaxies of the SDSS finding similar trends to those obtained by T04. G05 observed that both age and metallicity tend to increase with stellar mass, showing a rapid growth at intermediate masses and a gradual flattening above $M_* \sim 10^{10.35}$ $M_\odot\ h^{-1}$. Recently, Savaglio et al. (2005) estimated a relative evolution of 0.10–0.15 dex at $z \approx 0.7$ with respect to the local MZR of T04 while Erb et al. (2006a) found a relative evolution of ≈0.30 dex for the MZR of galaxies at $z \approx 2.5$.

The understanding of the origin of the LZR and MZR within the context of the current cosmological paradigm can provide more stringent constrains for galaxy formation models since these correlations are produced by the intervening action of different physical processes. In this scenario, galaxies formed by the hierarchical aggregation of substructures which can affect the internal distribution of angular momentum and mass in galaxies, modifying the star formation rate and the metal production and distribution. SN energy feedback is also expected to play a main role by contributing to establish a self-regulated star formation activity and to trigger powerful outflows. Finally, the interaction between a galaxy and its environment (i.e. groups or clusters) may strip gas, starving galaxies and quenching the star formation activity and the synthetization of new chemical elements.

Numerical simulations which can describe the non-linear evolution of the matter and its chemical enrichment self-consistently have proved to be an adequate tool to tackle galaxy formation (Lia & Carraro 2001; Mosconi et al. 2001; Kawata & Gibson 2003). In particular, Tissera, De Rossi & Scannapieco (2005) used chemical hydrodynamical simulations to show that galaxy-like systems in the concordance ΛCDM model followed the general trend of the observed MZR, predicting an evolution in zero-point and slope. The authors also claimed the need for strong SN galactic winds to decrease the fraction of metals locked into stars, specially in low-mass systems. Although SN energy feedback has been regarded as a crucial physical mechanism to regulate the star formation activity in galaxies and to produce metal-loaded, gas outflows capable of enriching the intergalactic medium, its modelling within hydrodynamical simulations is still controversial. For this reason, in this work we analyse in more detail the origin of both the LZR and the MZR and study the properties of the simulated galaxies with the aim at improving our understanding of the evolution of both relations in a hierarchical scenario, focusing on the role of dynamics. A secondary goal of our work is to clarify where and how SN energy feedback is required. A full study including SN energy feedback will be carried out in the future when the SN model of Scannapieco et al. (2006) gets fully tuned to be used in cosmological simulations.

This paper is organized as follows. Section 2 summarizes the main characteristics of the simulations. Section 3 provides a description of the simulated galaxies and an analysis of their mean astrophysical properties. Section 4 and Section 5 discuss the simulated fundamental metallicity relations and their evolution. Section 6 investigates the origin of the characteristic stellar mass. And Section 7 summarizes our main results.

2 NUMERICAL SIMULATIONS

We run numerical hydrodynamical simulations consistent with the concordance Lambda cold dark matter (ΛCDM) universe with $\Omega = 0.3$, $\Lambda = 0.7$, $\Omega_b = 0.04$ and $H_0 = 100\,h^{-1}$ km s^{-1} Mpc^{-1} with $h = 0.7$. These simulations were performed by using the chemical GADGET-2, which includes a treatment for metal-dependent radiative cooling, stochastic star formation and chemical enrichment (Scannapieco et al. 2005).

The chemical GADGET-2 code describes the enrichment by Type II and Type Ia supernovae (SNII and SNIa) according to the chemical yield prescriptions of Woosley & Weaver (1995) and Thielemann, Nomoto & Hashimoto (1993), respectively. Instantaneous thermalization of the SN energy has been assumed in this work. Previous works have shown that the injection of SN energy directly into the internal energy of the gas has no impact on the dynamics, so in our model SN energy feedback is inefficient (see Marri & White 2003 for a comprehensive review). We adopted a standard Salpeter initial mass function (IMF) with a lower and upper mass cut-offs of 0.1 and 40 $M_\odot$, respectively. For SNIa we assumed a time-delay for the ejection of material randomly chosen within [0.1, 1] Gyr. We assumed instantaneous recycling condition for SNII. Metals are distributed within the neighbouring gas particles weighted by the smoothing kernel. For more details on the chemical model, the reader is referred to Scannapieco et al. (2005).

The simulated volume corresponds to a cubic box of a comoving 10 Mpc h^{-1} side length. We ran two experiments resolved initially with 2×160^3 (S160) and 2×80^3 (S80) particles, respectively. Hence, the mass resolutions considered are of 2.17×10^7 $M_\odot\ h^{-1}$ (S80) and 2.71×10^6 $M_\odot\ h^{-1}$ (S160) for the gas component, and 1.41×10^8 $M_\odot\ h^{-1}$ (S80) and 1.76×10^7 $M_\odot\ h^{-1}$ (S160) for dark matter.

3 SIMULATED GALAXIES

The identification of the simulated galaxies was carried out by combining the friends-of-friends technique and a contrast density criterion which selects virialized structures as described by White, Efstathiou & Frenk (1993). In order to diminish numerical resolution problems, we only analysed those systems with virial masses greater than $\sim 10^9$ $M_\odot\ h^{-1}$. In S160, the analysed simulated galaxies are then required to have more than 2000 particles within the virial radius, while systems in S80 have at least 200 particles. Hence, our results are valid for galaxies with masses larger than this cut-off mass. The comparison between results from S80 and S160 will allow us to assess the effects of numerical resolution on the results.

In order to perform a better comparison with observations, the star formation histories as well as mean dynamical and chemical properties of the simulated galaxies are estimated at the optical radius $r_{\rm opt}$, defined as the one which encloses 83 per cent of the baryonic mass of the system. The typical $r_{\rm opt}$ for the simulated systems identified at $z = 0$ ranges within [2, 20] kpc h^{-1}, with the mean value at ∼6 kpc h^{-1}. For the sake of comparison with observations, we also estimate the aperture radius $r_{\rm ap}$ as the one that encloses 33 per cent of the baryonic mass of the system. This radius will be used to estimate mean abundances for a direct comparison with observational data.

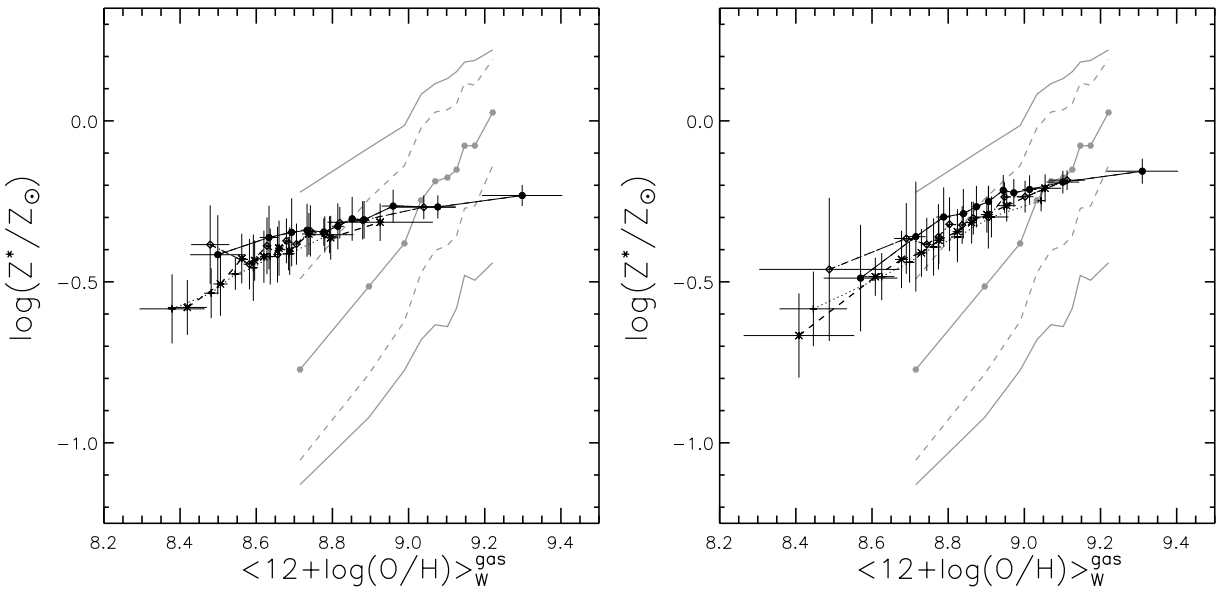

Figure 1. Mean stellar metallicity Z^* and gas O/H abundance for simulated galaxies at $z = 3$ (dotted line), $z = 2$ (dashed line), $z = 1$ (dot–dashed line) and $z = 0$ (solid line), considering the mass enclosed by $r_{\rm opt}$ (left-hand panel) and $r_{\rm ap}$ (right-hand panel). The error bars denote the rms deviations about mean values. The grey filled circles show the median stellar metallicity for the sample of SDSS galaxies analysed by G05, while the outer solid lines show the corresponding 16th and 84th percentiles. The dashed lines indicate the mean 68 per cent confidence range in the stellar metallicity estimated.

3.1 Chemical properties

Our simulations provide the abundances of several individual chemical elements such as ^{16}O, ^{56}Fe, H, etc., present in baryons as a result of stellar evolution. In particular, we can directly examine indicators such as the mean oxygen abundance, $12 + \log(\mathrm{O/H})$. However, the confrontation of the simulated results with observations may be tricky since, besides several observational difficulties related to the determination of chemical abundances, some observed estimators could be biased towards high star formation regions (e.g. estimations for H II regions) or the central part of galaxies (e.g. estimations from SDSS). Hence, depending on the observational data chosen to carry out a comparison, aperture effects must be taken into account, for example.

We define the mean mass-weighted O/H indicator as

$$\langle 12 + \log(\mathrm{O/H})\rangle_{\rm W} = 12 + \log\left(\frac{\sum_{i=1}^{N_{\rm p}} \mathrm{O}_i}{\sum_{i=1}^{N_{\rm p}} \mathrm{H}_i}\right), \quad (1)$$

where O_i and H_i are the oxygen and hydrogen atomic abundances in particle i and $N_{\rm p}$ corresponds to the total number of particles within an optical radius (or the aperture radius). This indicator can be easily estimated for the gas and stellar components in a given simulated galaxy.

G05 have recently obtained a positive correlation between O/H abundance of the gas phase and the stellar metallicity Z^* (i.e. total mass of all elements heavier than helium over the total stellar mass) for a sample of star-forming galaxies of the SDSS. In Fig. 1 (left-hand panel), we show this relation for the simulated galaxies at different redshifts. Although the simulated abundances are within a range of values consistent with those obtained by G05 at $z = 0$, the simulated relation is shallower than that estimated for the SDSS galaxies.

Taking into account that the SDSS provides information of the central regions of galaxies defined by the aperture angle, in order to evaluate at which level aperture effects could be responsible for this discrepancy, we estimated the stellar metallicity Z^* and O/H gas phase abundance within $r_{\rm ap}$. The results are shown in Fig. 1 (right-hand panel). We see that, limiting our metallicity estimations to the central region of galactic systems leads to a steeper correlation in better agreement with observations. Nevertheless, there is still a discrepancy which may be owing to the lack of strong energy feedback in our numerical model, which might have a direct impact on the chemical enrichment of the matter, principally, for low-mass systems (see e.g. Scannapieco et al. 2006).

Regarding the evolution of this relation with redsfhit, from Fig. 1 (right-hand panel), we can see that, at a given gas phase metallicity and albeit the high dispersion, galactic systems tend to have systematically more enriched stars at low redshift. Our simulations predict a mild evolution (i.e. less than 0.10 dex) in the correlation between stellar metallicity Z^* and gas phase abundance from $z = 3$ to 0 which is, nevertheless, within the estimated standard dispersion.

Finally, as noted by Tissera et al. (2005), the abundances of the gas phase have a large dispersion which introduces important noise to the estimated relation. For this reason, these authors decided to use the abundances estimated from the stellar populations to assess the level of evolution in the MZR. In this paper, we use both indicators for the comparison with observations. But chemical indicators estimated by using the stellar populations will be used for the rest of the discussions since the signals and noise are significantly smaller.

We tested that numerical resolution is not strongly affecting these determinations by analysing the results from S80 run which are found to be consistent with those of S160. Hereafter, for the sake of simplicity we will show only the results for S160 but simulated galaxies in S80 determine similar relations and results.

3.2 Gas fractions and masses

Gas fractions in galaxies are the result of the combined effects of the rate of transformation of gas into stars, gas infall and outflows. Mergers and interactions may help to increase the rate of accretion and to strip material from the systems, playing a role in the

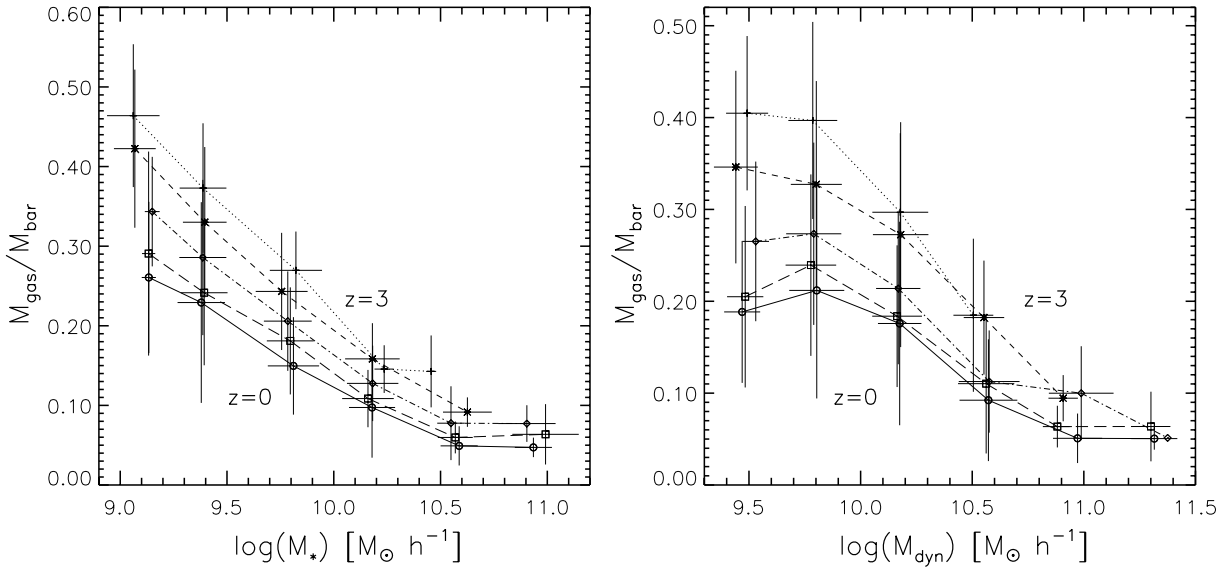

Figure 2. Gas mass normalized to total baryonic mass within the optical radius as a function of stellar mass (left-hand panel) and dynamical mass (right-hand panel) for simulated galaxies at $z = 3$ (dotted line), $z = 2$ (dashed line), $z = 1$ (dot–dashed line), $z = 0.5$ (long-dashed line) and $z = 0$ (solid line). The error bars correspond to the rms deviations about the mean values.

regulation of the star formation activity. Local observations show an anticorrelation between gas fraction and luminosity (e.g. Boselli et al. 2001) or stellar masses (Brinchmann & Ellis 2000). Recently, Erb et al. (2006b) reported hints for a similar relation at $z \sim 2$–2.5. Moreover, these authors found a mean $M_{\rm gas}/M_{\rm bar} \sim 0.50$ while T04 measured a mean of 0.20 for galaxies at $z \sim 0$. This trend illustrates the transformation of gas into stars with time. Since in our simulations, the gas reservoirs in the simulated galaxies are determined by the interplay between gas infall and star formation activity, which are both regulated by the hierarchical assemble of the structure, it is interesting to analyse at what extent the mentioned observational results can be reproduced by our simulations.

Hence, we estimated the gas fraction in the simulated galaxies as a function of stellar mass from $z \sim 3$ to $\sim$0 as displayed in Fig. 2 (left-hand panel). The fraction of gas increases for higher redshifts, with the largest changes for the smallest systems. At the low stellar mass end, the dispersion in the gas fraction is quite large, indicating that these systems have different evolutionary histories. Galactic systems with $M_* > 10^{10}$ M$_\odot$ h^{-1} have already consumed most of their gas into stars at $z > 3$. While at $z = 0$, we found mean $M_{\rm gas}/M_{\rm bar}$ varying between $\sim$0.20 and $\sim$0.05, at $z \sim 2$ mean values are in the range 0.10–0.40. These latest gas fractions are lower by a factor of $\sim$2 than the mean one reported by Erb et al. (2006b). This finding suggests again the need for strong SN winds to regulate the transformation of gas into stars as the systems are assembled. The lack of strong SN winds results in our findings being upper limits for the fraction of stars that systems can form at different redshifts as a result of their dynamical evolution in hierarchical scenarios. However, we also note that Erb et al. (2006b) assumed a Chabrier IMF while in our simulations, we adopted a Salpeter IMF, fact that leads to an overestimation by up to a factor of $\sim$2 of the fraction of baryons locked into stars. The different IMFs could account for these differences between the simulated and observed gas fractions.

According to Fig. 2 (left-hand panel), there is a variation of a factor of 5 in gas fraction over a change in 2 dex in stellar mass. It will be interesting to see if the same trend holds if dynamical masses are used instead of stellar masses. This is indeed the case, as shown in Fig. 2 (right-hand panel), although the relation is flatter for lower dynamical masses owing to the contribution of systems with different gas fractions at a given dynamical mass. Dynamical masses are calculated taking into account all baryons and dark matter within an optical radius.

Observations predict a good correlation between stellar and dynamical masses (e.g. Brinchmann & Ellis 2000). We found this tight correlation from $z \approx 3$, as it can be seen from Fig. 3 (upper panel). There is a small change in the slope of the relation from $z = 3$ to 0. This behaviour can be also understood from Fig. 3 (lower panel) where we show the ratio between dynamical and stellar mass as a function of stellar mass. On average, the hierarchical growth of the structure produces systems with dynamical masses a factor of 2.0–2.5 higher than their mean stellar mass since $z \sim 3$. This trend is consistent with that recently reported by Erb et al. (2006b) from observations of galaxies at $z = 2.0$–2.5. In the simulations, the anticorrelation is produced by the fact that smaller systems have a larger fraction of baryons in the form of gas at all redshifts. For lower redshifts, the slope of the relation changes because small systems continuously transformed their gas components into stars while larger systems increase slightly their dark matter content within an optical radius. This last behaviour was determined by estimating the fraction of each mass component (i.e. gas, stars and dark matter) within an optical radius for all systems as a function of redshift.

4 THE LUMINOSITY–METALLICITY RELATION

The magnitudes for our simulated galaxies have been estimated by applying the technique described by Tissera, Lambas & Abadi (1997) which combines the information on the stars generated by the simulations and population synthesis models. In particular, we use the models of Bruzual & Charlot (in preparation), which enables the determination of the spectral properties for stellar populations with different levels of enrichment. The integrated-light of simulated galaxies were estimated by convolving the age and chemical content of each simulated stellar population (represented by a star particle)

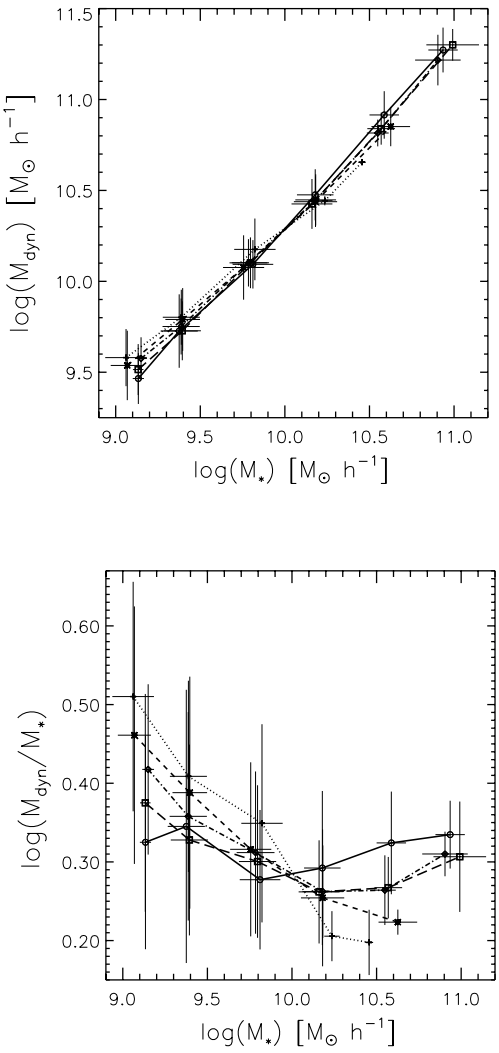

Figure 3. Dynamical mass versus stellar mass (upper panel) and the ratio between dynamical and stellar mass as function of stellar mass (lower panel) estimated at the same redshifts quoted in Fig. 2. The error bars correspond to the rms deviations about the mean values.

with the corresponding synthetic spectrum generated by Bruzual & Charlot (in preparation) models, according to

$$F_\lambda = \sum_j m_j \, F(\lambda, Z_j, t_j) \, f_{\rm ext}(\lambda, \tau_V, t_j) \qquad (2)$$

where m_j, t_j and Z_j correspond to the mass, the age and the metallicity of star j, respectively. The function F depicts the flux at a wavelength λ for a star with a given age and metallicity, while $f_{\rm ext}$ is introduced in order to describe the attenuation by dust and is defined following the work of Charlot & Fall (2000) as

$$f_{\rm ext}(\lambda, \tau_V, t_j) = {\rm e}^{-\tau_\lambda(\lambda, \tau_V, t_j)} \qquad (3)$$

where τ_V is the total optical depth in the V band affecting young stars. The relation between τ_λ and τ_V is given by the extinction curve, which describes the attenuation due to photons emitted in all directions by stars of age t_j in a galaxy. Charlot & Fall (2000) consider a scenario in which stars form in interstellar clouds and after 10^7 yr emigrate towards the interstellar medium, deriving an extinction curve with the form

$$\tau_\lambda(\lambda, \tau_V, t) = \begin{cases} \tau_V \, (\lambda/5500 \text{ Å})^{-0.7} & \text{if } t \leqslant 10^7 \text{ yr} \\ \mu \, \tau_V \, (\lambda/5500 \text{ Å})^{-0.7} & \text{if } t > 10^7 \text{ yr} \end{cases}, \qquad (4)$$

where μ is an adjustable parameter which represents the fraction of the total optical depth contributed by the interstellar medium.

In this work we consider a random distribution of μ along the range [0, 0.6] as suggested by Bruzual & Charlot (in preparation). For τ_V, we use recent observational results which suggest that it may be a function of the metallicity of the galaxy. To estimate this last correlation we made a polynomial fit to the observed correlation obtained from the SDSS (Brichmann, private communication) and assumed Gaussian uncertainties. With this model we determined the spectral properties of galaxies and derived colours and magnitudes.

At $z = 0$ we found that the simulated galaxies determine an LZR relation in general good agreement with observations as it can be appreciated from Table 1 where we show the results of the linear regression fits to the simulated relation in the B band. For comparison we also include the corresponding fit for the SDSS galaxies reported by T04. We used the B band so that these results can be confronted with observational works where this bandwidth is often used.

Table 1. Parameters for the linear regressions of the local LZR: $12 + \log({\rm O/H}) = b + aM_B$. The errors are shown in parentheses.

Sample	$12 + \log({\rm O/H}) = b + aM_B$ b	a
Simulated stellar component	7.74 (0.07)	−0.06 (0.01)
Simulated gas phase	8.73 (0.22)	−0.01 (0.01)
T04	7.74	−0.05 (0.01)

Observational results suggest an evolution in the zero-point and slope of the LZR (Kobulnicky & Koo 2000; Pettini et al. 2001; Kobulnicky et al. 2003; Lilly, Carollo & Stockton 2003; Kobulnicky & Kewley 2004; Maier et al. 2004; Shapley et al. 2004), so that, at a given metallicity, on average, galaxies are brighter at higher redshifts. To study the evolution of the simulated LZR, we estimated this relation at several redshifts and performed linear regression fits through the data. In Fig. 4, we show the results of these fits for the mass-weighted oxygen indicators for the stars (upper panel) and gas components (lower panel) at the four redshifts of interest. We also include mean values estimated in magnitude bins of equal point number. Table 2 summarizes the fitting parameters for all analysed redshifts. As it can be appreciated from Fig. 4, a linear regression is a good representation of the data. The results show that the simulated LZRs evolve in such a way that systems become more metal-rich with time, at a given luminosity. The major changes are detected at the fainter end of the relation. This evolution is not only true at a fix magnitude but also for individual galaxies which tend to become fainter in M_r with time. Moreover, our simulations indicate that, at given metallicity, simulated galaxies are, at least, 3 mag brighter at $z \sim 3$ than systems at $z = 0$ (see Shapley et al. 2004). We estimate a mean overall change of $\approx$0.15 dex in the chemical content of the simulated galaxies from $z \sim 1$ (see Kobulnicky & Kewley 2004). Note that the LZR estimated from the gas-phase abundances have shallower slopes than those estimated from the stellar components, mainly because of the high level of noise.

We stress the difficulties involved in the confrontation of observations with simulations owing to different uncertainties affecting the estimations of both observed and simulated luminosities. Taking into account the growing body of evidences that the fundamental

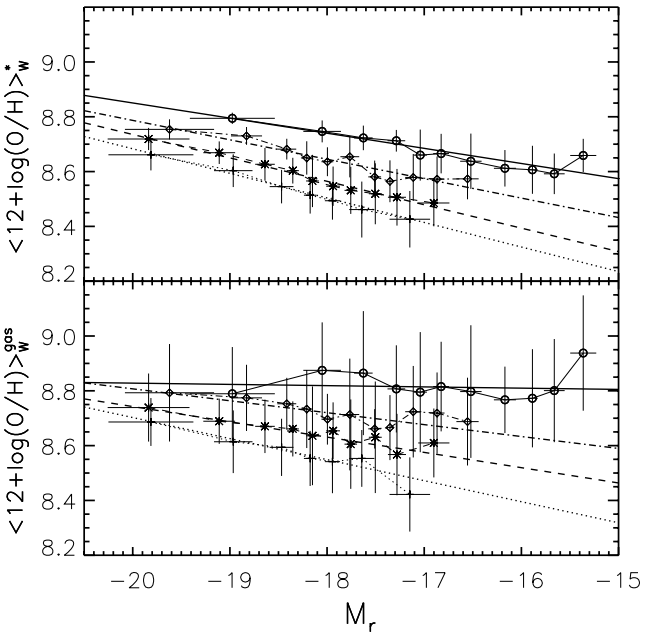

Figure 4. The LZR for the stellar component (upper panel) and the gas-phase (lower panel) of simulated galaxies identified at $z = 3$ (dotted line), $z = 2$ (dashed line), $z = 1$ (dot–dashed line) and $z = 0$ (solid line). The error bars denote the rms deviations in bins of equal point number.

Table 2. Parameters for the linear regressions of the simulated LZR relations: $12 + \log(O/H) = b + aM_r$ as a function of redshift.

	Stellar component		Gas phase	
z	b	a	b	a
4.00	6.671 ± 0.239	-0.098 ± 0.013	7.059 ± 0.305	-0.077 ± 0.017
3.50	7.024 ± 0.179	-0.081 ± 0.010	7.210 ± 0.214	-0.072 ± 0.012
3.00	6.891 ± 0.130	-0.090 ± 0.007	7.167 ± 0.202	-0.077 ± 0.011
2.50	6.750 ± 0.125	-0.099 ± 0.007	7.113 ± 0.200	-0.081 ± 0.011
2.00	7.026 ± 0.117	-0.085 ± 0.006	7.627 ± 0.185	-0.056 ± 0.010
1.80	7.259 ± 0.109	-0.074 ± 0.006	7.695 ± 0.184	-0.053 ± 0.010
1.50	7.220 ± 0.108	-0.077 ± 0.006	7.643 ± 0.179	-0.057 ± 0.010
1.30	7.414 ± 0.094	-0.067 ± 0.005	8.136 ± 0.192	-0.031 ± 0.011
1.00	7.369 ± 0.092	-0.071 ± 0.005	7.937 ± 0.184	-0.044 ± 0.010
0.80	7.366 ± 0.091	-0.072 ± 0.005	8.227 ± 0.214	-0.028 ± 0.012
0.50	7.629 ± 0.076	-0.059 ± 0.004	8.639 ± 0.214	-0.008 ± 0.012
0.12	7.651 ± 0.066	-0.060 ± 0.004	8.604 ± 0.226	-0.012 ± 0.013
0.00	7.744 ± 0.070	-0.055 ± 0.004	8.736 ± 0.218	-0.005 ± 0.013

relation is between metallicity and stellar mass, we will hereafter concentrate on the analysis of the MZR.

5 THE STELLAR MASS–METALLICITY RELATION

New observational results are starting to provide information on the stellar mass and metallicity of galaxies not only at $z = 0$ but in the intermediate (Savaglio et al. 2005) and high-redshift (Erb et al. 2006a) universe. Despite the large observational difficulties to reliably estimate metallicities and stellar masses at high redshift, a general picture, suggesting evolution, is starting to appear. In fact, taking into account the detailed discussion presented by Savaglio et al. (2005) and Erb et al. (2006a), a relative evolution of 0.1–0.15 dex at $z \sim 0.7$ and of $\sim$0.30 dex at $z \sim 2$ has been determined.

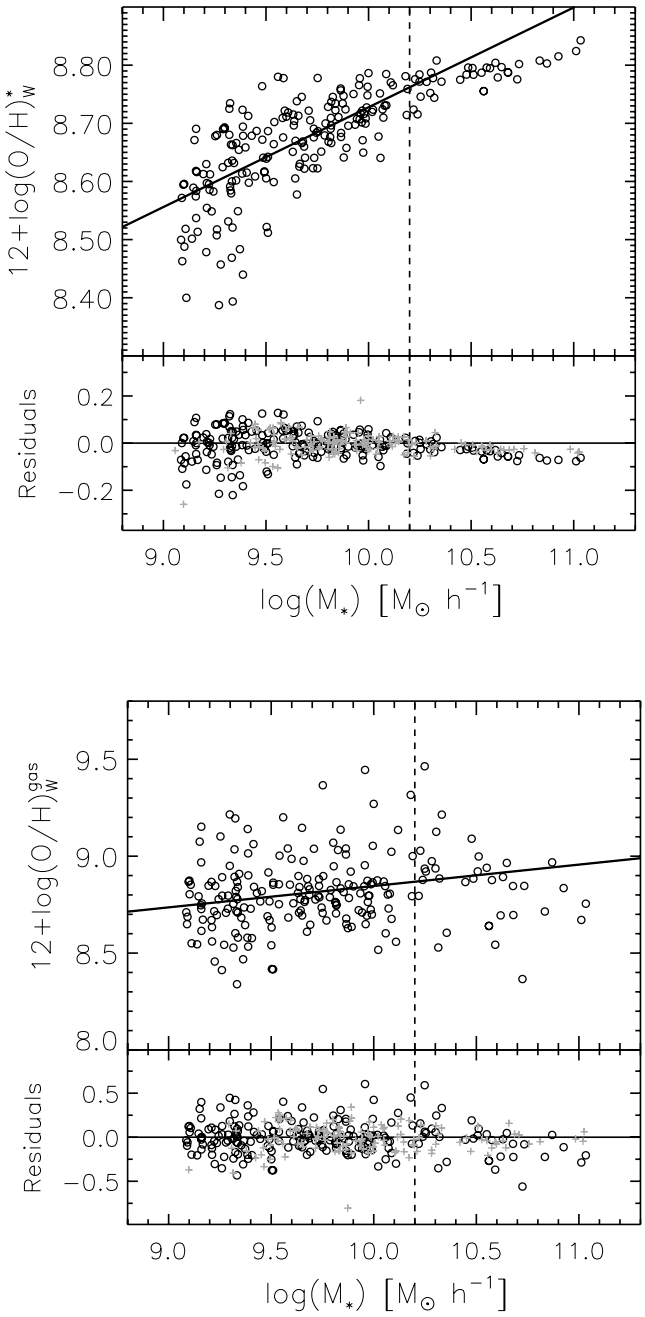

Figure 5. MZR at $z = 0$ obtained for the stellar component (upper panel) and gas-phase (lower panel) at r_{opt}. Linear fits to the relations are also shown (solid line) for comparison. The dashed line indicates the characteristic stellar mass where the residuals of the linear fits (lower panels) to the stellar MZR start to systematically depart from zero. In the lower panel the circles depicts S160 and the crosses S80.

In the case of simulations, the estimation of the MZR is direct. The upper panel of Fig. 5 shows the simulated local MZR using the stellar, mass-weighted O/H abundance as an indicator while the lower panel displays the MZR estimated by using the gas abundances. It is clear that the gas abundances have much larger dispersion. We carried out linear regression fits to both distributions (solid lines). As it can be appreciated from this figure, a linear regression through the data does not provide a good representation of the simulated abundances for the whole range of stellar masses. In small lower

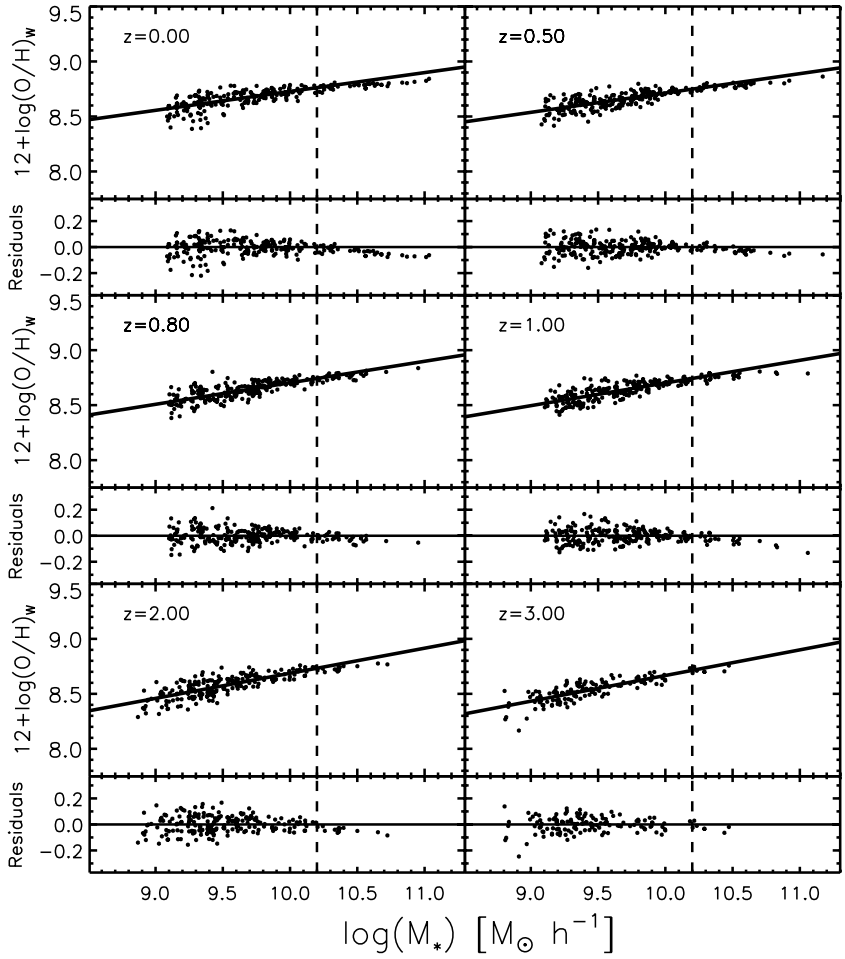

Figure 6. The MZR for simulated galaxies at different redshifts and the residuals (small boxes) estimated with respect to linear regression fits (solid lines). The dashed lines indicate the characteristic stellar mass where the residuals start to systematically depart from zero.

panels we displayed the residuals of these relations. As it can be seen from these distributions, for stellar masses larger than $M_c \approx 10^{10.2}\,M_\odot\,h^{-1}$, the residuals become systematically negative, indicating a flattening of the slope for systems with larger stellar masses. A slight higher $M_c(\approx 10^{10.4}\ M_\odot\,h^{-1})$ is suggested from the abundances in gas phase distribution. However, due to the high dispersion present in the gas-phase data, we take $M_c \approx 10^{10.2}\,M_\odot\,h^{-1}$ as the reference mass. We have also included the same estimations for the simulated galaxies in S80 (grey crosses) in order to assess the effects of resolution in the determination of M_c. As it can be seen both simulations (which differ by approximately an order of magnitude in mass resolution) yield similar results.

Interestingly, this stellar mass M_c is not far from the characteristic mass $\approx 10^{10.5}\,M_\odot\,h^{-1}$ determined by Kauffmann et al. (2004), which is claimed by these authors to separate spheroid-dominated galaxies from spiral-dominated ones. T04 also determined that their MZR changes curvature at approximately the same stellar mass. Hence, the fact that this characteristic mass is also found in our simulations suggests that the way in which building blocks are assembled might play a relevant role in its determination.

In order to make a more direct comparison of our data with observations (see also Section 5.1), we also estimated M_c by computing the mean oxygen abundance within r_{ap} and the residuals of the linear fits to the resulting MZRs. We obtained that limiting our analysis to the central region of galaxies shifts the characteristic M_c of the stellar MZR to $\approx 10^{10.3}\,M_\odot\,h^{-1}$ and that of the gas phase one to $\approx 10^{10.5}\,M_\odot\,h^{-1}$, approaching the observed value. However, it is important to note that if Kauffmann et al. (2004) or T04 had assumed a Salpeter IMF, their characteristic mass would have been about 0.2 dex higher and hence even higher than the one obtained from simulations.

In order to investigate the origin of the MZR and the M_c, we estimated this relation as a function of redshift. In the case of M_c, we used the MZR estimated from the stellar abundances because of their lower dispersion with respect to those obtained from the gas abundances and measured at r_{opt}. These abundances provide a better estimation of the characteristics of the galaxies to study their chemical evolution. From Fig. 6, we observe that the MZR exhibits the same general patterns from $z = 0$ to 3, but with a displacement towards larger abundances for decreasing redshift. In the small panels of Fig. 6, we show the residuals of each relation with respect to the corresponding linear regression fit. As we can appreciate, at all analysed redshifts, we find the same behaviour: the residuals become systematically negative for $M_* > M_c$.

The characteristic mass remains almost unchanged from $z = 3$, with an evolution of its abundance by only 0.05 dex in the same redshift range. As discussed by Tissera et al. (2005), the major variations in the chemical content are found for systems with $M_* < M_c$

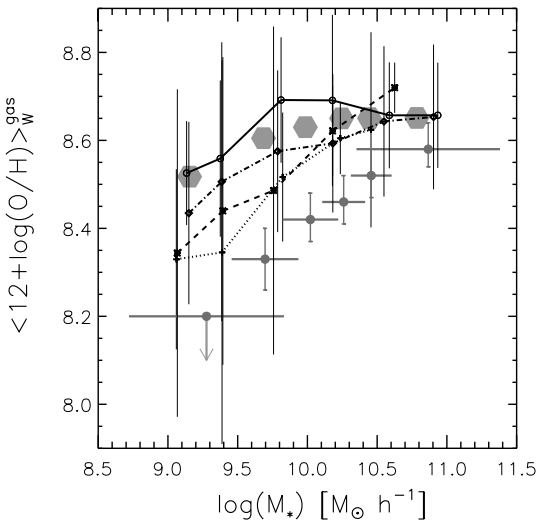

Figure 7. The gas-phase MZR for simulated galaxies at different redshifts (see Fig. 4 for line code). The oxygen abundances are calculated at r_{ap}. Filled circles denote the observed MZR at $z \sim 2$ by Erb et al. (2006a) while the large hexagons correspond to the observed MZR at $z = 0$ by T04 as recalculated by Erb et al. (2005a). Note that we have displaced the simulated MZRs by -0.26 dex in order to fit the gas-phase abundances of T04 at low stellar masses and that this displacement roughly agrees with that estimated by Erb et al. (2005a) for the T04 relation.

which, on average, increase their abundances by ≈0.20 dex from $z \sim 3$ to ∼0. Systems with $M_* > M_c$ show an increase in the level of enrichment of ≈0.05 dex in the same redshift range. Note that even at $z > 2$, galaxies with $M_* > M_c$ can have stellar populations with mean solar abundances.

From Fig. 6 we can also appreciate that, at a given stellar mass, the dispersion in oxygen abundances increases for higher redshift, and that the dispersion is larger for smaller stellar mass systems. The different evolution found for simulated galaxies of different masses and the dependence of the dispersion on stellar mass are produced by their different evolutionary paths which establish the way the systems are assembled and how the gas is consumed into stars in these simulations where SN feedback has not been included yet.

5.1 Comparison with observations

As discussed by Tissera et al. (2005), the level of evolution obtained in the metallicity content of the simulated galaxies in models without feedback is weaker than that suggested by recent observations. These authors chose the mean O/H abundances in the simulated stellar populations to estimate the MZR because of the high dispersion present in the gas abundances. In order to improve the comparison with observations, in this section we will use the gas abundances estimated at the aperture radius (r_{apt}) to assess the evolution predicted by our model. This is because the SDSS explored only the central regions of galaxies enclosing approximately 1/3 of the luminosity of the galaxies.

In Fig. 7 we plot the simulated MZR from $z = 3$ to 0 (see also Tables 3 and 4), the observations of Erb et al. (2006a) and the observed MZR of T04 as obtained by Erb et al. (2006a) by using their own metallicity estimator. Erb et al. (2006a) performed a detailed comparison between both sets of observations, concluding that an evolution of 0.30 dex from $z \approx 2$ to 0 could be reliably claimed. The simulated MZR has been shifted by -0.26 dex in order to fit the observational MZR of T04 for low-mass systems, as the metallicity indicator employed by Erb et al. (2006a) saturates at higher metallicities and cannot be trusted, according to those authors. Note that the displacement applied to the simulated MZR at $z \sim 0$ is consistent with the global displacement estimated by Erb et al. (2006a) for the MZR of T04. Hence, at $z \sim 0$ our simulated MZR calculated at r_{apt} agrees with that of T04 without requiring any extra correction.

Table 3. Mean simulated gas-phase O/H abundances estimated within r_{ap} for different stellar mass bins at $z = 3.0$, 2.0, 1.0, 0.8, 0.5, 0.0. The number N of galaxies identified at each redshift is also shown.

M_* ($M_\odot\ h^{-1}$)	$\langle 12 + \log(O/H)\rangle$					
$\log(M_*) < 9.20$	8.59 ± 0.20	8.60 ± 0.37	8.69 ± 0.21	8.79 ± 0.12	8.82 ± 0.17	8.79 ± 0.12
$9.20 \leqslant \log(M_*) < 9.60$	8.61 ± 0.44	8.70 ± 0.35	8.77 ± 0.32	8.82 ± 0.18	8.79 ± 0.47	8.82 ± 0.18
$9.60 \leqslant \log(M_*) < 10.00$	8.78 ± 0.15	8.75 ± 0.37	8.84 ± 0.18	8.95 ± 0.14	8.91 ± 0.15	8.95 ± 0.14
$10.00 \leqslant \log(M_*) < 10.40$	8.87 ± 0.08	8.88 ± 0.10	8.85 ± 0.16	8.95 ± 0.19	8.89 ± 0.14	8.95 ± 0.19
$10.40 \leqslant \log(M_*) < 10.80$	8.88 ± 0.22	8.98 ± 0.06	8.90 ± 0.17	8.92 ± 0.12	8.89 ± 0.13	8.92 ± 0.12
$10.80 \leqslant \log(M_*)$	–	–	8.91 ± 0.16	8.92 ± 0.12	8.90 ± 0.12	8.92 ± 0.12
z	3.00	2.00	1.00	0.80	0.50	0.00
N	137	202	241	239	239	227

Table 4. Mean simulated stellar O/H abundances estimated within r_{ap} for different stellar mass bins at $z = 3.0$, 2.0, 1.0, 0.8, 0.5, 0.0. The number N of galaxies identified at each redshift is also shown.

M_* ($M_\odot\ h^{-1}$)	$\langle 12 + \log(O/H)\rangle$					
$\log(M_*) < 9.20$	8.40 ± 0.34	8.46 ± 0.26	8.52 ± 0.15	8.56 ± 0.10	8.58 ± 0.08	8.62 ± 0.08
$9.20 \leqslant \log(M_*) < 9.60$	8.49 ± 0.29	8.55 ± 0.29	8.62 ± 0.13	8.59 ± 0.28	8.66 ± 0.11	8.66 ± 0.14
$9.60 \leqslant \log(M_*) < 10.00$	8.65 ± 0.10	8.65 ± 0.14	8.71 ± 0.07	8.69 ± 0.12	8.72 ± 0.07	8.75 ± 0.10
$10.00 \leqslant \log(M_*) < 10.40$	8.77 ± 0.02	8.76 ± 0.06	8.78 ± 0.04	8.76 ± 0.08	8.80 ± 0.03	8.80 ± 0.06
$10.40 \leqslant \log(M_*) < 10.80$	8.79 ± 0.01	8.82 ± 0.03	8.81 ± 0.03	8.76 ± 0.12	8.83 ± 0.02	8.83 ± 0.02
$10.80 \leqslant \log(M_*)$	–	–	8.82 ± 0.04	8.89 ± 0.00	8.89 ± 0.04	8.87 ± 0.03
z	3.00	2.00	1.00	0.80	0.50	0.00
N	137	202	241	239	239	227

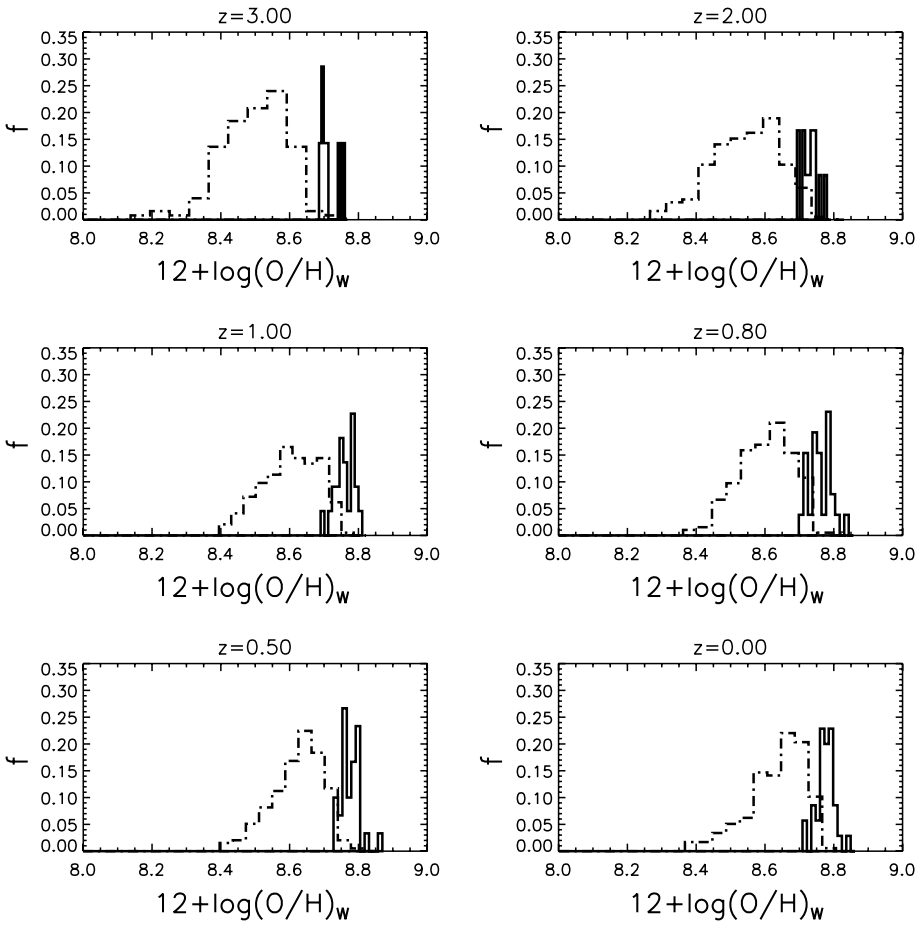

Figure 8. Mass-weighted oxygen abundance distributions of the stellar populations for galaxy-like systems with $M_* < M_c$ (dot–dashed lines) and $M_* > M_c$ (solid lines) at different redshifts.

As it can be appreciated, in the simulations, we found a lower level of evolution in comparison with observations, with a change of ≈0.05 dex for the high stellar mass end and ≈0.1–0.15 dex for the low stellar mass end. From this figure, we can see that a better agreement between simulations and observations seems to require SN winds in order to decrease the metallicity content not only for low stellar mass systems but also for large stellar masses. This last issue is still controversial because, as reported by Erb et al. (2006), their metallicity indicator could be saturated for high metallicities and hence, the authors do not assure that the level of evolution they reach for larger masses is, actually, correct. Also, in the simulations and observations, different IMFs have been adopted, fact that introduces an uncertainty in the determination of the stellar mass of up a factor of 2, among them.

6 DISCUSSION

In order to understand the physical meaning of the evolution of the MZR and of the characteristic mass, M_c, we have analysed the merger trees of the simulated systems at $z = 0$ and the variation of the astrophysical properties along the evolutionary paths.

6.1 Does M_c segregate two different types of galaxies?

In previous sections, we investigated the relation between the metal content of the simulated galaxies in a ΛCDM scenario and their dynamical and astrophysical properties finding that the chemical enrichment of systems increase with luminosity and stellar mass. When estimating the MZR as a function of redshift, we detected a characteristic stellar mass ($M_c \sim 10^{10.2}\,M_\odot\,h^{-1}$) at which the relation changes curvature towards a flatter slope. This M_c seems to be approximately constant with redshift, reaching solar abundance at $z \approx 0$ but with an overall chemical evolution of only ≈0.05 dex since $z \approx 3$.

Interestingly, the simulated M_c agrees with a similar motivated stellar mass determined by Tremonti et al. (2004) in an observational study of the MZR for galaxies in the SDSS-DR2. It is also worth noting the consistency of M_c with the characteristic mass derived by Kauffmann et al. (2004) when analysing the astrophysical properties of galaxies in SDSS. Note that the simulated M_c can vary in the range $10^{10.5}$–$10^{10.2}$ depending on the region where abundances are estimated (i.e. r_{opt} and r_{ap} and on the adopted metallicity estimator (i.e. gas or stellar metallicities). Kauffmann et al. (2004) found that galaxies with large stellar masses tend to be dominated by old stars, in spheroid-type systems with red colours, while smaller systems determine a different galaxy population with their astrophysical properties corresponding to younger, blue, disc-dominated galaxies. In this section, we assess if M_c can separate the simulated galaxies into two different populations.

In Fig. 8 we show the distributions of O/H abundances of the stellar populations in the simulated galaxies separated into two groups depending on their stellar mass. Massive systems ($M_* > M_c$) have

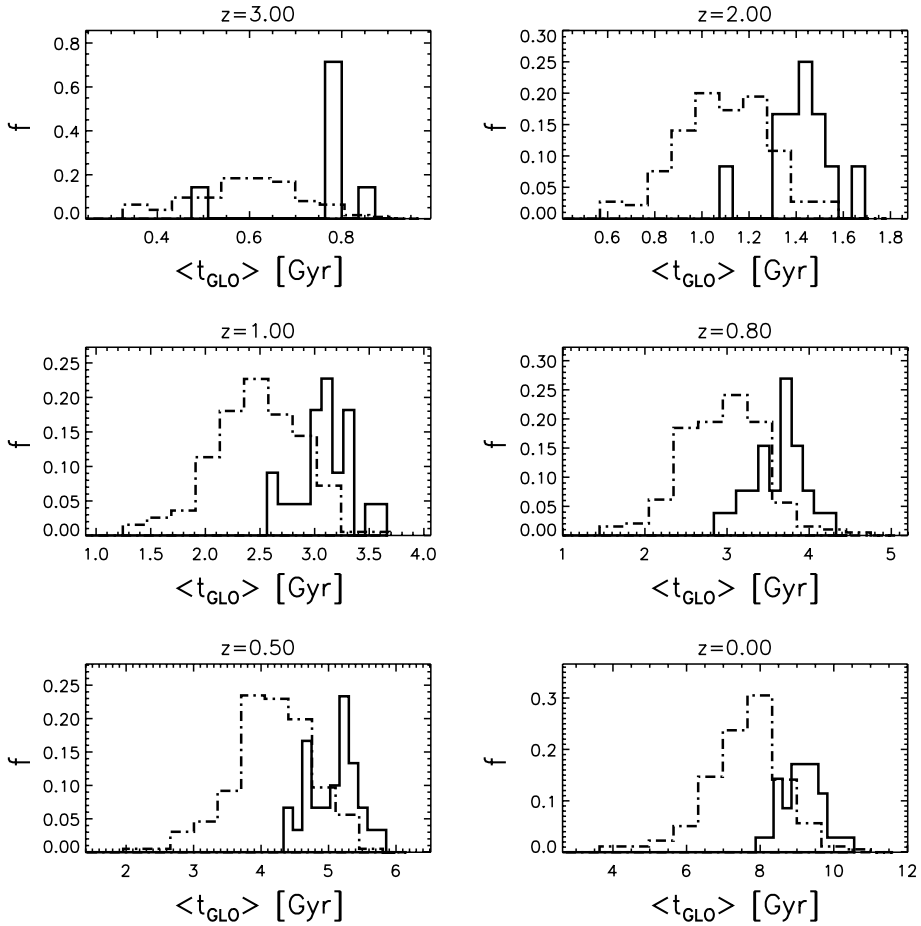

Figure 9. Distributions of the mean ages of stellar population in simulated galaxies with $M_* < M_c$ (dot–dashed lines) and with $M_* > M_c$ (solid lines) at different redshifts.

mean abundances comparable to solar levels from $z \sim 3$. The distributions are quite narrow (with a width of ≈0.10 dex) indicating that the composition of the stellar populations in these systems are very similar even at $z \sim 3$, experiencing no significant changes in the analysed redshift range. Conversely, simulated galaxies with $M_* < M_c$ show a broader metallicity distribution which evolves to higher level of enrichment with redshift.

The fact that massive systems are dominated by old stellar populations can be confirmed by inspecting Fig. 9 where we show a similar plot to that of Fig. 8 but as a function of the mean stellar age of the simulated galaxies. As it can be appreciated, massive systems have always mean older populations than the rest of the simulated systems. Again, smaller systems show a broader distribution with some of them having mean ages comparable to those of massive ones. However, the bulk of the stellar population in systems with $M_* < M_c$ is clearly younger than their massive counterparts.

These figures show that M_c segregates two distinctive galaxy populations with different histories of formation. The simulated massive galaxies are dominated, on average, by older and more metal-rich stellar populations than smaller systems. By combining metallicity and age information with the population models of Bruzual & Charlot (in preparation), we estimated colours as a function of redshift. As we can observe from Fig. 10, M_c also segregates galaxies into two clear colour distributions, with massive systems in the red tail of the distribution, even from $z \sim 3$. This finding is in agreement whit recent observational results obtained from the VIMOS-VLT Deep Survey of galaxies at $z \sim 2$ (Franzetti et al. 2006). In these simulations, blue and red colours which produce the bimodal distribution are determined by the star formation history of the systems which establishes the relative fraction of old to new stars and their metallicities. We note that the bimodal distribution at $z = 0$ is not in full agreement with observations (Balogh et al. 2004), principally because we are lacking a fraction of very red systems ($u - r > 2$). There are two possible reasons for this. First, it is possible that the action of SN feedback could contribute to modulate a bimodal colour distribution in full agreement with that observed at $z = 0$. Secondly, the small volume simulated in this work could prevent us from reproducing the complete range of observed colours.

These trends show that in these simulations M_c segregates two different galaxy populations in a similar sense to the trend reported by Kauffmann et al. (2004). Our results also indicate that M_c remains as a characteristic mass up to $z \approx 3$. Our findings suggest that the origin of M_c can be directly linked to the way the structure is built up in a hierarchical universe. SN feedback is expected to play a relevant role in the regulation of the star formation activity. However, this process might not significantly affect the M_c as we will discuss in the next section.

6.2 The hierarchical building up of the structure

From the analysis of the merger trees, we find that systems with $M_* < M_c$ transform their gas content into stars in a more passive

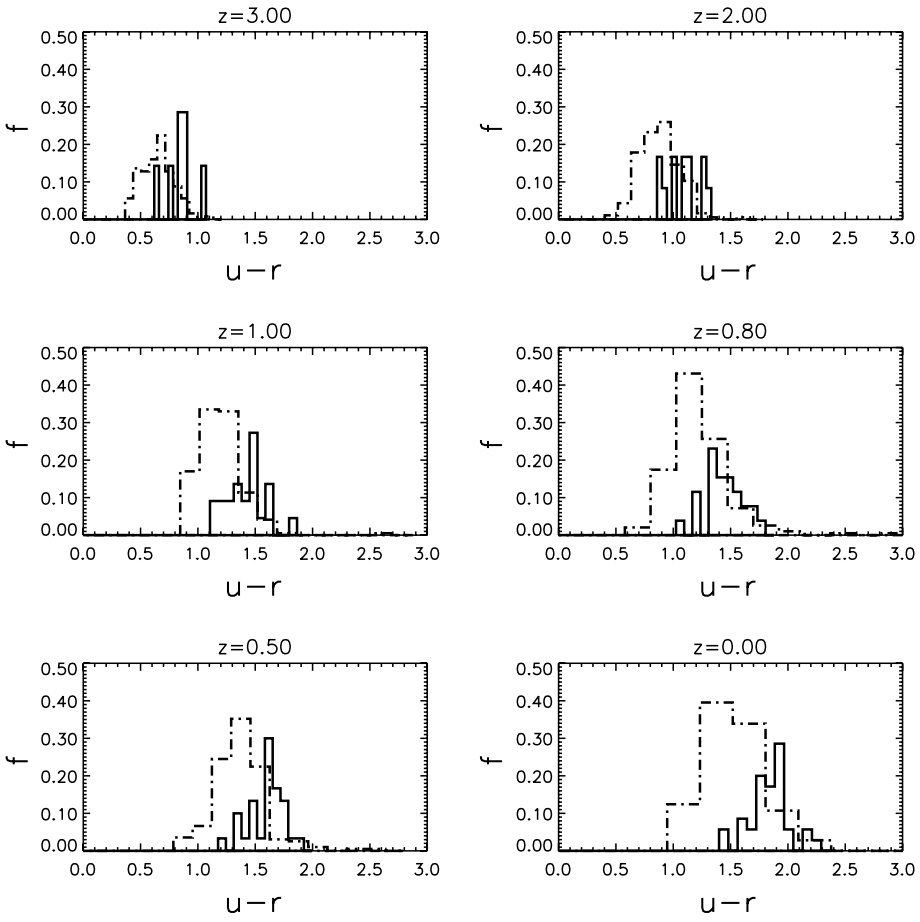

Figure 10. $u - r$ colour distributions in simulated galaxies with $M_* < M_c$ (dot–dashed lines) and with $M_* > M_c$ (solid lines) at the redshifts of interest.

fashion or via gas-rich mergers, setting a steeper correlation between stellar mass and metallicity (Tissera et al. 2005). In this case, the fraction of newborn stars in merger events is high enough so that the mean metallicity of the remanent systems is affected by the new stellar contribution.

Galaxies with masses larger than M_c are preferentially assembled by merger events which involve stellar dominated systems, with small leftover gas. In these cases, the mergers produce systems with final stellar masses equal to the sum of the old dominating stars plus some newborn ones, while its overall mean abundance remains at the same level of enrichment. This situation occurs because, in this case, the merging systems have already transformed most of their gas into stars so that there is no fuel for an important starburst during the merger. It could be also possible that a large system merges with a smaller less-enriched one which can feed new star formation activity but with lower level of enrichment. Both scenarios have the same flattening effect on the slope of the MZR in systems within this range of masses. We also estimated the fraction of gas in the simulated galaxies as a function of their stellar mass from $z \approx 3$. From this analysis, we found that systems with $M_* \sim M_c$ have, on average, 15 per cent of leftover gas (Fig. 2) at all analysed redshifts.

How stars in systems of different masses are formed can be seen in Fig. 11 where we show the fraction of stellar mass in the simulated galaxies identified at $z = 0$ which formed at different z. As it can be appreciated from this plot, simulated galaxies with $M_* > M_c$ have 50 per cent of their stars formed at $z \geqslant 1.5$ with less than 30 per cent

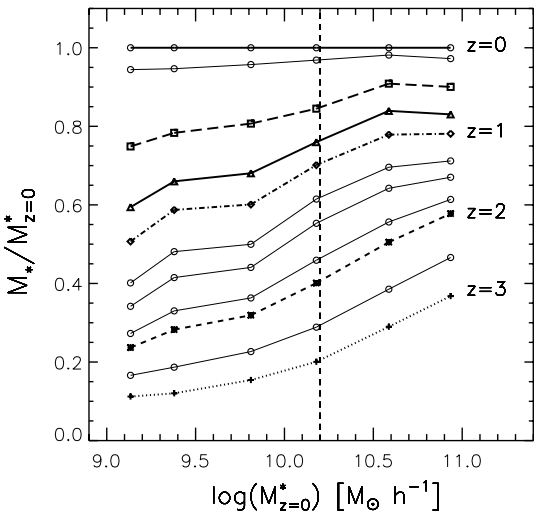

Figure 11. Fraction of total stellar mass in simulated galaxies at $z = 0$ formed at different redshifts. From bottom to top the lines correspond to $z = 3.0, 2.5, 2.0, 1.8, 1.5, 1.3, 1.0, 0.8, 0.5, 0.1, 0.0$.

appearing after $z \approx 1$. In the case of simulated galaxies with $M_* < M_c$, they have 50 per cent of the stars formed after $z \approx 1.3$. Note that these stars would probably belong to different substructures which then merged to build up our simulated galaxies at $z = 0$. In other

words, our results do not imply that a given simulated galaxy at $z = 0$ was formed at certain redshift, but that a given fraction of its stars was born at that time. These stars could have belonged to different substructures by the redshift of reference. The ensemble of the final systems can occur at lower redshift resulting in a natural 'downsizing' scenario (see also De Lucia et al. 2006; Neistein, van den Bosch & Dekel 2006).

6.3 The missing process: SN energy feedback

As we mentioned before, we have not included an effective SN energy feedback treatment in our simulations, which is expected to produce powerful outflows, affecting the star formation process and the metal production and mixing. Taking into account theoretical results, the effects of SN feedback depend strongly on the potential well of the systems and is expected to affect mainly systems with circular velocities smaller than 100 km s^{-1} (e.g. Larson 1974). The simulations analysed in the paper do not include a strong SN energy feedback that can actually produce an impact on the dynamical evolution and star formation activity of the systems (Scannapieco et al. 2006). Nevertheless, we can assess the effects we would expect.

In Fig. 12 we show the MZR (upper panel) and velocity–metallicity relation (VZR; lower panel) from $z = 3$ to 0. The optical velocity has been estimated as $V_{\rm opt} = [GM\ (r < r_{\rm opt})/r_{\rm opt}]^{0.5}$ where $M\ (r < r_{\rm opt})$ is the total mass within the optical radius, $r_{\rm opt}$. Hence, $V_{\rm opt}$ is a measure of the potential well of the system.

From this figure it can be appreciated that the chemical content of the simulated galaxies tends to increase with optical velocities. Fast rotating systems increase their chemical abundances by $\sim$0.10 dex from $z = 3$ to 0, while at lower velocities the variations are of $\sim$0.25 dex. From these figures, we can see how, on average, at a certain stellar mass, systems become slower rotators and more chemical enriched with decreasing redshift. At a given circular velocity, the evolution in metallicity is larger since, at lower redshift, systems of larger stellar masses contribute to this given circular velocity. The VZR shows a higher level of evolution with redshift than the MZR as a consequence of the combination of metallicity enrichment and cosmology. The increase of the mean density of the universe at higher redshift produces that, at a given stellar mass, systems need to be more concentrated in order to get gravitationally bounded and separate from the general expansion. Then, for a given stellar mass the virialization of the system occurs at higher circular velocities for higher redshift.

Assuming that SN energy feedback will affect more strongly slow rotating systems (i.e. Larson 1974; Dekel & Silk 1986), we expect that the $M_{\rm c}$ may not be strongly modified by this process. This is because, as seen in Fig. 12, the optical velocity corresponding to $M_{\rm c}$ varies from around 300 km s^{-1} at $z = 3$ to 140 km s^{-1} at $z = 0$. However, because the hierarchical aggregation of the structure, large systems might be affected through the strong action of SN energy feedback in the substructure that merged to form them.

It is clear that since the strongest effects of SN energy feedback are expected to take place in the small mass range, the excess of metals in the MZR shown by Tissera et al. (2005) could be solved by this process. The action of strong SN feedback would produce the ejection of part of the enriched material out of the systems and the decrease of the general level of enrichment making the slope of the simulated MZR for $M_* < M_{\rm c}$ steeper as we expect from the observational relation.

The need for SN outflows is also suggested by the analysis of the effective yields [defined as $y_Z = Z/\ln(\mu)^{-1}$ where Z is the gas-phase metallicity and μ the gas fraction of the systems], as shown

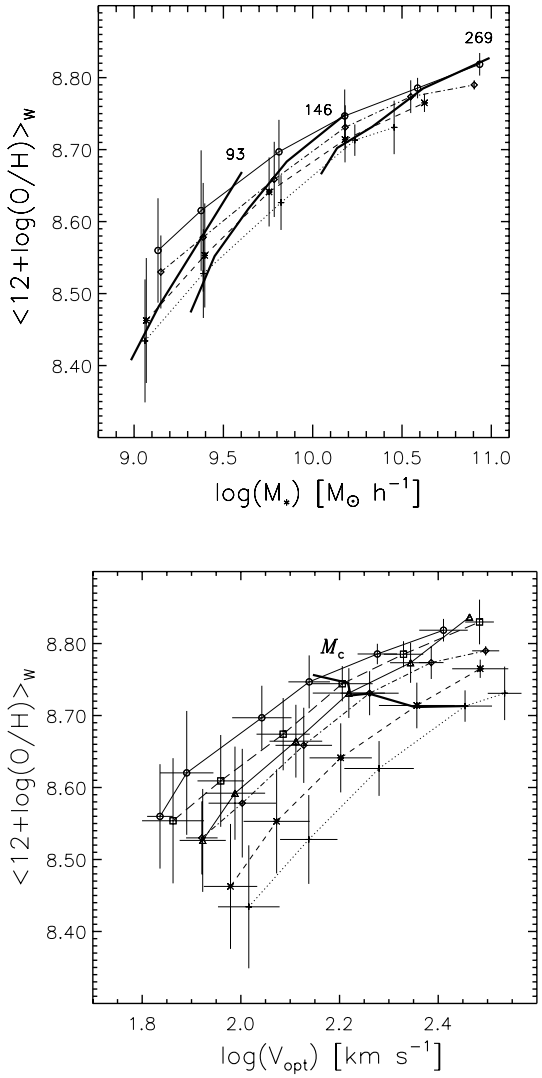

Figure 12. Mean MZR (upper panel) and VZR (lower panel) for galactic systems at $z = 3$ (dotted line), $z = 2$ (dashed line), $z = 1$ (dot–dashed line) and $z = 0$ (solid line). Upper panel: The thick solid lines represent curves of constant optical velocities (93 km s^{-1}, 146 km s^{-1} and 269 km s^{-1}). Lower panel: the thick solid line depicts the line of constant $M_{\rm c}$. Results at $z = 0.5$ (long-dashed line) and $z = 0.8$ (triple-dot–dashed line) are also shown. The error bars correspond to s.d. values estimated in bins of $\sim$0.4 dex in log M_*. Note that the VZRs for $z = 3$ and 2 do not have the bin corresponding to the largest stellar mass interval owing to the lack of a statistical number of systems with high stellar mass at very high redshift in our simulated volume.

in Fig. 13 for the simulated galaxies at $z = 0$. These abundances were estimated within $r_{\rm apt}$ in order to mimic the aperture effects previously discussed. The simulated y_Z values are lower than the solar yield expected in a closed box model, since our systems formed in a hierarchical scenario where mergers, interactions and infall affect the mass distribution and regulate star formation. Contrary to observations (e.g. Garnett 2002), we found larger y_Z for systems with $10^9\,{\rm M}_\odot\,h^{-1} < M_* < M_{\rm c}$ compared to those of the massive ones ($M_* > M_{\rm c}$), which supports the claim for stronger SN outflows for the former. In the case of massive systems, we get a mean of y_Z which remains approximately constant with optical velocity. Although this latest result is in agreement with Garnett (2002), it might be indicating the need for some ejection of material also in massive systems

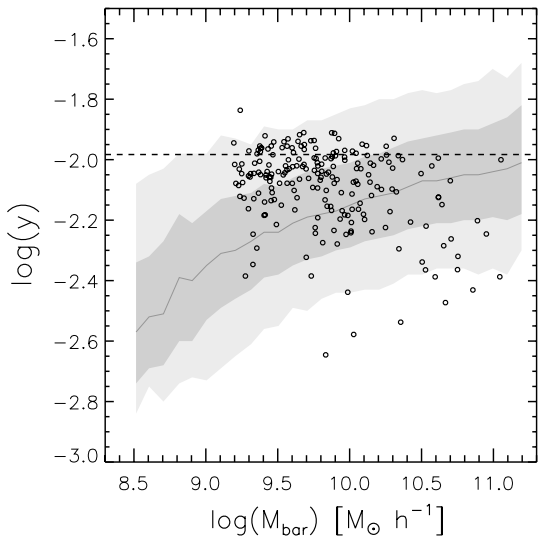

Figure 13. Effective yields as a function of baryonic mass for the simulated galaxies at $z = 0$. The shaded area corresponds to the estimations of T04 for galaxies in SDSS. The dashed line represents the solar value.

in the light of the new observational findings of T04, who claimed to find a weak trend for all systems.

7 CONCLUSIONS

In this paper, we studied the dynamical, astrophysical and chemical properties of simulated galaxies in a hierarchical clustering scenario consistent with the concordance ΛCDM model. In this scenario, systems grew by the aggregation of smaller ones, generating correlations between luminosity, stellar mass, circular velocity and metallicity which are in general agreement with observations. Our main goal was to underpin the effect of the hierarchical assembly of galaxy building blocks on the metallicity fundamental relations. The non-linear formation of the structure makes complex the understanding of how star formation, gas cooling and accretion, mergers and environmental effects work together and of the impact they have on the determination of relations between dynamical and metallicity properties.

We found that the cooling and transformation of gas into stars inside substructures that grow hierarchically results in the determination of a characteristic mass which segregates systems dominated, on average, by old, red and metal-rich stellar populations from those more gas-rich and dominated by young stars. The characteristic mass arises because the formation of large systems is produced by the fusion of substructures dominated by old stellar populations with a small fraction of newborn stars associated to the merger events. This behaviour generates a change in the slope of the MZR since the outcomes of mergers are larger systems with approximately the same mean abundances. On the other hand, less massive systems tend to form their stars in a more passive way or by rich-gas mergers leading to a more strong correlation between stellar mass and metallicity. This characteristic stellar mass agrees with that obtained by Kauffmann et al. (2004) from the analysis of galaxies in the SDSS-DR2. Nevertheless, the simulated evolution of the MZR is milder than present observational evidence. Strong SN energy feedback could help to reconcile models and observations.

Our results suggest that this M_c remains unchanged since $z = 3$ playing the role of segregating galaxies into these two distinctive populations. Systems with stellar masses smaller than M_c are the ones experiencing the largest changes in their astrophysical properties since $z \approx 3$. These systems are responsible for the evolution of the LZR so that at a given metallicity, simulated systems are found to be around 3 mag brighter at high redshift. Small simulated galaxies constitute a diverse population which has formed approximately 50 per cent of their stars since $z \approx 1$. Conversely, large systems had half their stars formed at $z > 2$, on average.

Our results suggest that in the concordance cosmology, the hierarchical aggregation of the structure, which regulates the gas infall and the star formation activity in the absence of energy feedback, is a key process which can dynamically determine a characteristic stellar mass M_c. The simulated M_c plays a similar role to that of the characteristic mass obtained from observations. Certainly, SN feedback is also expected to play an important role in shaping the MZR as already shown by previous works such as Larson (1974) and Chiosi & Carraro (2002). However, it is accepted that the effects of SN feedback depend on the potential well of the systems. In hierarchical scenarios, this is an important aspect since the formation of galaxies may have involved the aggregation of substructures with a wide range of masses, each of them susceptible to be differentially affected by SN energy feedback (depending on their virial masses). Then, to probe the effects of SN feedback, it is of utmost importance which histories of formation are assumed for galaxies. In this work, we provide galaxy formation histories consistent with the concordance models. Within this context, our findings suggest that since $z = 3$, SN feedback might have a weak effect on M_c, owing to the fact that this characteristic mass corresponds to fast rotating systems even at $z = 0$. However, this point will be adequately discuss in a forthcoming paper.

ACKNOWLEDGMENTS

The authors are grateful to the anonymous referee for the detailed and thoughtful comments that help to improve this paper and to A. Gallazzi for making available their data in electronic form. This work was supported in part by Consejo Nacional de Investigaciones Científicas y Técnicas, Agencia de Promoción de Ciencia y Tecnología and Fundación Antorchas from Argentina. PBT thanks the Aspen Center for Physics during the 2004 Summer Workshop for useful discussions that help to the development of this work. The simulations were performed on Ingeld PC Cluster hosted by the Numerical Astrophysics group at Institute of Astronomy and Space Physics. This work was partially supported by the European Union's ALFA-II programme, through LENAC, the Latin American European Network for Astrophysics and Cosmology.

REFERENCES

Balogh M. L., Baldry I. K., Nichol R., Miller C., Bower R., Glazebrook K., 2004, ApJ, 615, L101
Boselli A., Gavazzi G., Donas J., Scodeggio M., 2001, AJ, 121, 753
Brinchmann J., Ellis R. S., 2000, ApJ, 536, L77
Bruzual G., Charlot S., 2003, MNRAS, 344, 1000
Charlot S., Fall S. M., 2000, ApJ, 539, 718
Chiosi C., Carraro G., 2002, MNRAS, 335, 335
Cole S., Lacey C. G., Baugh C. M., Frenk C. S., 2000, MNRAS, 319, 168
De Lucia G., Springel V., White S. D. M., Croton D., Kauffmann G., 2006, MNRAS, 366, 499
Dekel A., Silk J., 1986, ApJ, 303, 39
Erb D. K., Shapley A. E., Pettini M., Steidel C. C., Reddy N. A., Adelberger K. L., 2006a, ApJ, 647, 128

Erb D. K., Shapley A. E., Pettini M., Steidel C. C., Reddy N. A., Adelberger K. L., 2006b, ApJ, 646, 107
Franzetti P. et al., 2006, preprint (astro-ph/0607075)
Freeman K., Bland-Hawthorn J., 2002, ARA&A, 40, 487
Gallazzi A., Charlot S., Brinchmann J., White S. D. M., Tremonti C. A., 2005, MNRAS, 362, 41 (G05)
Garnett D. R., 2002, ApJ, 581, 1019
Kauffmann G., Charlot S., 1998, MNRAS, 294, 705
Kauffmann G., White S. D. M., Heckman T. M., Ménard B., Brinchmann J., Charlot S., Tremonti C., Brinkmann J., 2004, MNRAS, 353, 713
Kawata D., Gibson B. K., 2003, MNRAS, 340, 908
Kobulnicky H. A., Kewley L. J., 2004, ApJ, 617, 240
Kobulnicky H. A., Koo D. C., 2000, ApJ, 545, 712
Kobulnicky H. A. et al., 2003, ApJ, 599, 1006
Lamareille F., Mouhcine M., Contini T., Lewis I., Maddox S., 2004, MNRAS, 350, 396
Larson R. B., 1974, MNRAS, 169, 229
Larson R. B., Dinerstein H. L., 1975, PASP, 87, 911
Lequeux J., Peimbert M., Rayo J. F., Serrano A., Torres-Peimbert S., 1979, A&A, 80, 155
Lia C., Carraro G., 2001, Ap&SS, 276, 1049
Lilly S. J., Carollo C. M., Stockton A. N., 2003, ApJ, 597, 730
Maier C., Meisenheimer K., Hippelein H., 2004, A&A, 418, 475
Marri S., White S. D. M., 2003, MNRAS, 345, 561
Mosconi M. B., Tissera P. B., Lambas D. G., Cora S. A., 2001, MNRAS, 325, 34
Neistein E., van den Bosch F. C., Dekel A., 2006, MNRAS, 372, 933
Pagel B. E. J., 1997, Nucleosynthesis and Chemical Evolution of Galaxies. Cambridge Univ. Press, Cambridge
Perez M. J., Tissera P. B., Scannapieco C., Lambas D. G., De Rossi M. E. 2006, A&A, in press (astro-ph/0605131)
Pettini M., 2006, in Le Brun, V., Mazure, A., Arnouts, S., Burgarella, D., eds, The Fabulous Destiny of Galaxies: Bridging Past and Present. Edition Frontières, Paris, in press
Pettini M., Shapley A. E., Steidel C. C., Cuby J.-G., Dickinson M., Moorwood A. F. M., Adelberger K. L., Giavalisco M., 2001, ApJ, 554, 981
Savaglio S. et al., 2005, ApJ, 635, 260
Scannapieco C., Tissera P. B., White S. D. M., Springel V., 2005, MNRAS, 364, 552
Scannapieco C., Tissera P. B., White S. D. M., Springel V., 2006, MNRAS, 371, 1125
Shapley A. E., Erb D. K., Pettini M., Steidel C. C., Adelberger K. L., 2004, ApJ, 612, 108
Somerville R. S., Primack J. R., 1999, MNRAS, 310, 1087
Springel V., Hernquist L., 2003, MNRAS, 339, 289
Thielemann F. K., Nomoto K., Hashimoto M., 1993, Origin and Evolution of the Elements. Cambridge Univ. Press, Cambridge
Tissera P. B., Lambas D. G., Abadi M. G., 1997, MNRAS, 286, 384
Tissera P. B., De Rossi M. E., Scannapieco C., 2005, MNRAS, 364, L38
Tremonti C. A. et al., 2004, ApJ, 613, 898 (T04)
White S. D. M., Rees M. J., 1978, MNRAS, 183, 341
White S. D. M., Efstathiou G., Frenk C. S., 1993, MNRAS, 262, 1023
Woosley S. E., Weaver T. A., 1995, ApJS, 101, 181

This paper has been typeset from a TEX/LATEX file prepared by the author.